Hindawi
Advances in Civil Engineering
Volume 2020, Article ID 1072161, 10 pages
https://doi.org/10.1155/2020/1072161

Research Article

Influence of "X" Fracture, Confining Pressure, and Temperature on Rock Masses' Failure Process

Yunjuan Chen,[1] Yi Jing,[1] Yanchun Yin,[2] Fuqiang Yin,[3] and Chenglong Zhao[1]

[1]*Civil Engineering College, Shandong Jianzhu University, Ji'nan 250101, China*
[2]*Key Laboratory of Mining Disaster Prevention and Control, Shandong University of Science and Technology, Qingdao 266590, China*
[3]*Shandong Provincial Institute of Land Surveying and Mapping, Ji'nan 250102, China*

Correspondence should be addressed to Yanchun Yin; yycrsd@163.com

Received 6 January 2020; Revised 4 August 2020; Accepted 20 October 2020; Published 2 December 2020

Academic Editor: Timo Saksala

Based on the similarity theory, sandstone was taken as the prototype, and rock-like specimens were made with the strength ratio of 1 : 1. Single "X" fracture and double "X" fractures were prefabricated in rock-like specimen, and crack propagation was studied through the compressive test. An improved discontinuous deformation analysis method (DDARF) was adopted to simulate on the cracking process. Further, other factors should not be ignored such as confining pressure and temperature, which were considered: rock's crack propagations under loading and unloading with different confining pressures were studied; influences of temperature from 20°C to 300°C on crack propagation were analyzed.

1. Introduction

Natural rock mass contains many discontinuities of different shapes and sizes. The existence of discontinuities greatly affects the mechanical and strength properties of rock mass [1–4]. Cross fracture is a common form of rock mass discontinuities in nature (see Figure 1). It is of great significance for rock engineering to analyze the rock failure process under compressive force [5–8]. Due to the limitation of experimental conditions and research methods, current studies are mainly focused on such discontinuities as single fracture, parallel fractures, intermittent fractures, caverns, or other holes in rock mass.

In recent years, some experts and scholars have gradually begun to pay attention to studies on cross fractures' crack propagation, and their researches have important guiding significance for rock mass engineering [9–13]. Li [14] studied the failure rule of rock-like specimen with trident fractures under uniaxial compression and analyzed its crack propagation form. Liu [15] carried out an experimental study on the crack propagation morphology of "T" fractures and single "X" fracture in rock-like specimen. Cao [16] investigated the macromechanical behavior and energy release mechanism of fractured rock-like specimens with cross nonpersistent fractures under uniaxial loading based on experimental tests and numerical simulation (PFC2D). These cross fractures are disconnected in the middle. Zhang [17–20] studied the failure mechanism by presetting the main and the secondary fracture of single cross fracture and analyzed the influence of anchorage position on the strength of fractured rock mass. In addition, some scholars [21–24] studied the migration of water flow in cross fractures and analyzed the seepage characteristics of rock mass.

On the basis of existing results, firstly rock-like specimens with cross fractures are made in this study, including not only the single "X" fracture, but also double "X" fractures. Secondly, the crack propagation of specimen's cross fracture is tested and studied under different conditions. At the same time, an improved discontinuous deformation analysis (DDARF) method is adopted to simulate the crack propagation process. Last but not least, influences of multi factors on the crack propagations of rock mass are comprehensively analyzed, including different temperatures (from room temperature to relative higher temperature) and different confining pressures under loading and unloading conditions.

Figure 1: Cross fractures in rock mass.

2. Failure Law of Rock-Like Specimen with Cross Fractures

The rock prototype is sandstone. After several materials' proportion optimization tests over and over again, sand, cement, water reducer, and water are finally selected as the rock-like materials with a mass ratio of 0.97 : 1 : 0.03 : 0.3. Among them, sand is the common river sand, using the four particle gradations of 1.18 mm, 0.6 mm, 0.3 mm, and 0.15 mm with the mass ratio of 1.33 : 1.11 : 1 : 1. The cement selected is the ordinary Portland cement (PO 42.5). Water reducer can play a role in reducing the amount of water and cement, reducing the setting time of cement mortar, and improving the plasticity of cement mortar. "X" fractures (cross fractures) are made by PVC sheet with a size of 0.5 mm $*$ 15 mm. After the rock-like specimens are made, they will need to be cured in the curing box for about two weeks, in order to get the steady physical and mechanical properties, and all are done; and these rock-like specimens can be loaded and analyzed as the real rock mass.

The production mold for rock-like specimen and "X" fracture is shown in Figure 2. Parts of the rock-like specimens prepared with single "X" fracture are shown in Figure 3.

Fifteen pieces of specimens are prepared for every "X" fracture angle (30° & 45°, 45° & 45° and 45° & 60°), and a conventional uniaxial loading test (GAW 2000) is carried out to analyze the failure process of the rock-like specimen. During the test, the specimen is firstly loaded by force until the specimen is in contact with the press plate completely, followed by displacement (0.1 mm/min), and its whole process is recorded in time. Failure mode of the rock-like specimen with single "X" fracture is shown in Figure 4.

As shown in Figure 4, the red fracture is the main one to crack, and it has the greater extent and scale of crack propagation, and the green one is the secondary. When the rock-like specimen has the "X" fracture angle of 45° & 45°, after the compressive loading, the two fractures have almost the same cracking extents, and their stress conditions are also basically the same, and of course both have the synchronized energy release, while when $\alpha \neq \beta$, that is to say, the two fracture angles of "X" fractures are not the same, such as 30° & 45° or 45° & 60°, the rock-like specimen's original equilibrium stress state is destroyed in the compressive loading process, and then the crack propagation and energy release will give priority to one of the two fractures. At the same time, we can see that, under axial compressive pressure, the cracking direction of rock-like specimen is almost parallel with the direction of maximum principal stress.

In order to verify the test results, an improved discontinuous deformation analysis (DDARF) method is adopted to simulate the failure process of these rock-like specimens. The improved DDARF [25–28] is put forward based on DDA (discontinuous deformation analysis method), and it can satisfy the basic elastic principle and has both the rigor of finite element method (FEM) and the calculation function of blocks' large displacement as discrete element method (DEM) [29–34]. DDARF is used to simulate the whole failure process for discontinuous rock mass, including crack initiation, propagation, penetration, and crushing. It must meet these three conditions: (1) displacement's complete first-order approximation; (2) equilibrium equation and minimum potential energy principle; and (3) no embedding and stretching blocks. The cracking algorithm of DDARF is that, firstly, lots of triangular blocks are generated by Traveling Wave Method in the numerical model; secondly, block's contact is divided into three types, where springs are used to ensure no stretching and no embedding (see Figure 5). Thirdly, block boundary is divided into real joint and virtual joint; when the virtual joint reaches its limit strength, the contact springs will be damaged, and rock's crack will propagate along the virtual joint. Thus, the virtual joint becomes the true joint, and its parameters will be reduced to real joint's parameters accordingly.

Simulation on the failure mode of rock-like specimen with single "X" fracture by DDARF is shown in Figure 6.

As shown in Figure 6, when the rock-like specimen has the "X" fracture angle of 30° & 45°, after the compressive loading, the crack propagation of fracture ① (30° fracture) is much slighter than that of fracture ② (45° fracture). When the rock-like specimen has the "X" fracture angle of 45° & 45°, after the compressive loading, the crack propagation of fracture ① (45° fracture) is similar to that of fracture ② (45° fracture). When the rock-like specimen has the "X" fracture angle of 45° & 60°, after the compressive loading, the crack propagation of fracture ① (60° fracture) is much slighter than that of fracture ② (45° fracture). So, the simulation results are in good agreement with the experimental results. When the two fractures have different angles, rock failure process will give priority to only one of the two, while when the two fractures have the same angles, they will propagate synchronously. Under this condition, wing cracks are generated and expanded firstly, and their sizes and numbers are much greater than those of secondary cracks.

Parts of the rock-like specimens made with double "X" fractures (their composition ratios and parameters are all the same) and their failure modes after the compressive loading are shown in Figure 7.

As seen from Figure 7(b), for specimens with double "X" fractures, after the compressive loading, about half of the specimens indicate that the upper set of "X" fracture plays the controlling role in cracking propagation, and energy releases

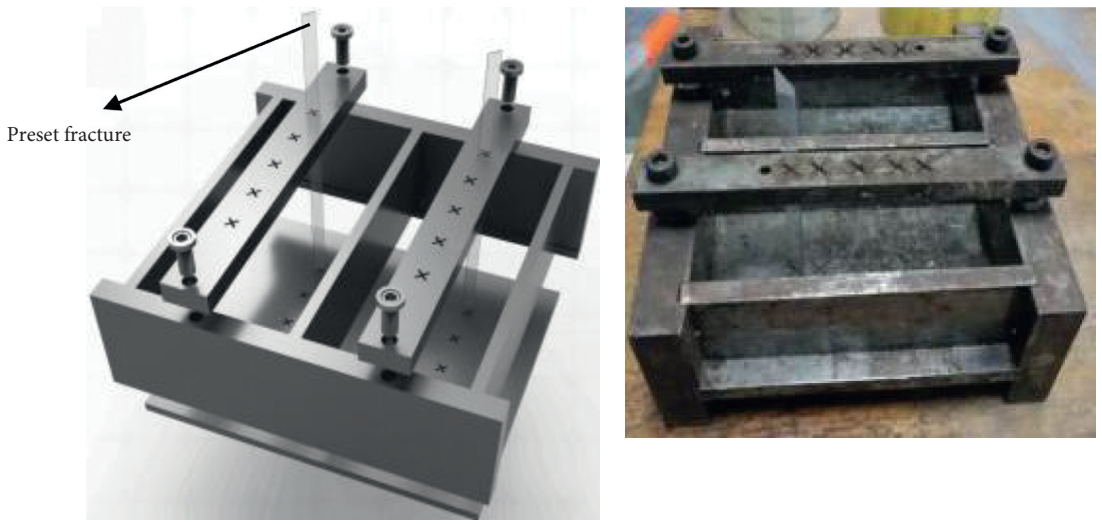

(a) (b)

Figure 2: Production mold for rock-like specimen with (a) three-dimensional sketchy map and (b) finished mold.

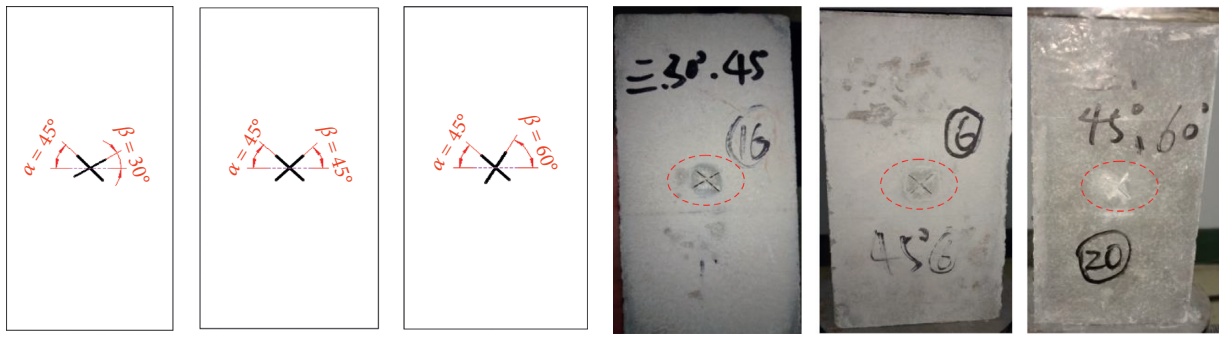

(a) (b)

Figure 3: Parts of rock-like specimens prepared with (a) sketchy map of "X" fracture specimen with different angles and (b) parts of single "X" fracture rock-like specimen prepared.

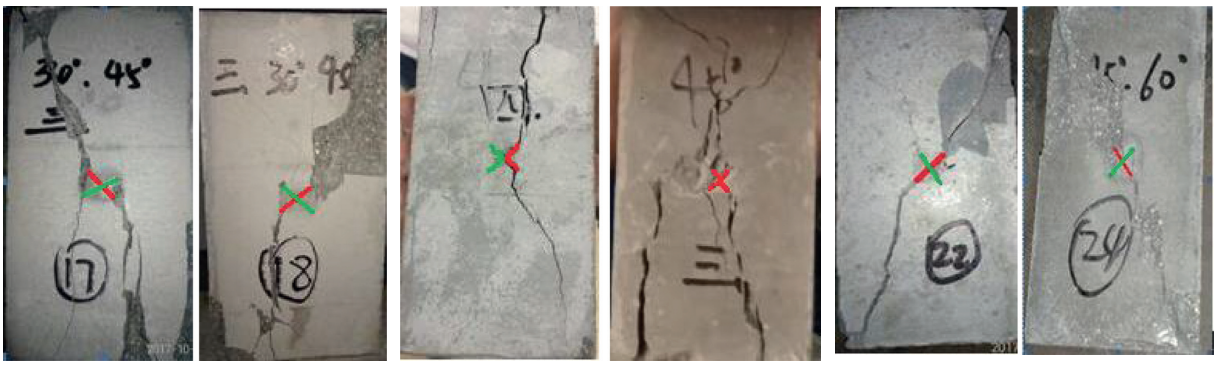

Figure 4: Failure mode of single "X" fracture specimen with different angles.

mainly through the upper set's cracking process, and thus to obtain the rock-like specimens' new equilibrium, just like specimens in the first line in Figure 7(b). And the other half of the specimens indicate that the lower set of "X" fracture plays the controlling role. In a word, if there are no other influence factors, for this kind of specimens, as long as one set of "X" fracture is selected as the breakthrough to release energy, the crack propagation will develop rapidly along this set. And, the

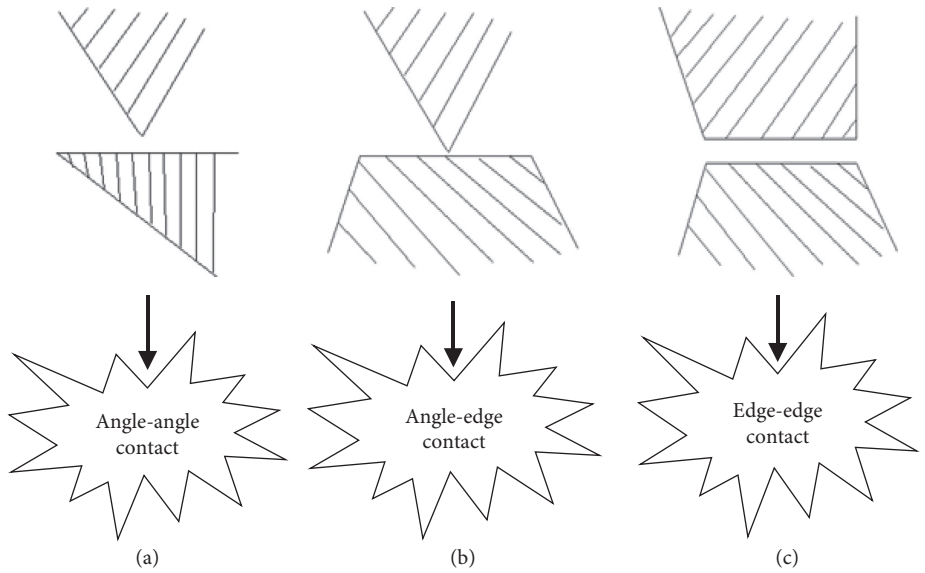

Figure 5: Block's contact of discontinuous deformation analysis for rock failure (DDARF). (a) Angle-angle contact. (b) Angle-edge contact. (c) Edge-edge contact.

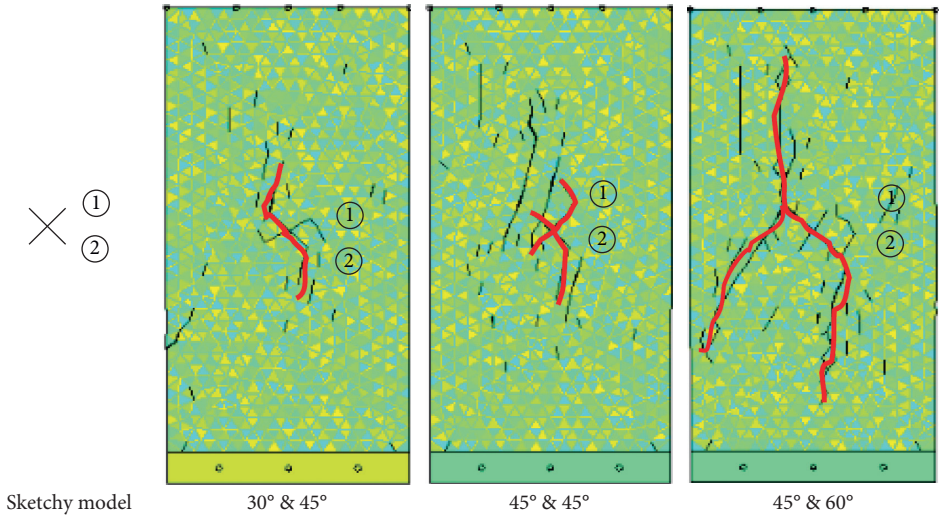

Figure 6: DDARF simulation on the failure mode of single "X" fracture specimen with different angles.

two sets of "X" fractures have the same opportunity to be selected as the controlling one.

As seen from Figure 8, the numerical simulation result is consistent with the experimental result. They all show that one of the two sets of "X" fractures will crack as the breakthrough point, and in the whole cracking process, it releases energy more greatly than the other set. And similar to the single "X" fractured specimen, here for two sets of "X" fractured specimen, wing cracks are also generated and expanded primarily.

3. Confining Pressure's Influence on Failure Law of Rock-Like Specimen

A triaxial loading machine developed by ourselves, with the high-precision multiway ultra-high pressure stepping proportional overflow valve hydraulic loading system, is used to apply the triaxial loading on the rock-like specimen, as shown in Figure 9. The loading precision of the system is up to 0.05 MPa, which can achieve smooth pressurization or decompression.

Using this self-developed loading machine, the influence of confining pressure on crack propagation of rock-like specimen is studied, and the test results are shown in Figure 10.

As shown in Figure 10, even though the same vertical load is applied on these rock-like specimens, the confining pressure is different, yet the cracking extent is different. Here, all the specimens are loaded with vertical force of 32 MPa. When the confining pressure is 0 MPa, the specimens are damaged greatly, and they have reached their peak strength. When the confining pressure is 5 MPa, there are two obvious cracks, and they do not reach

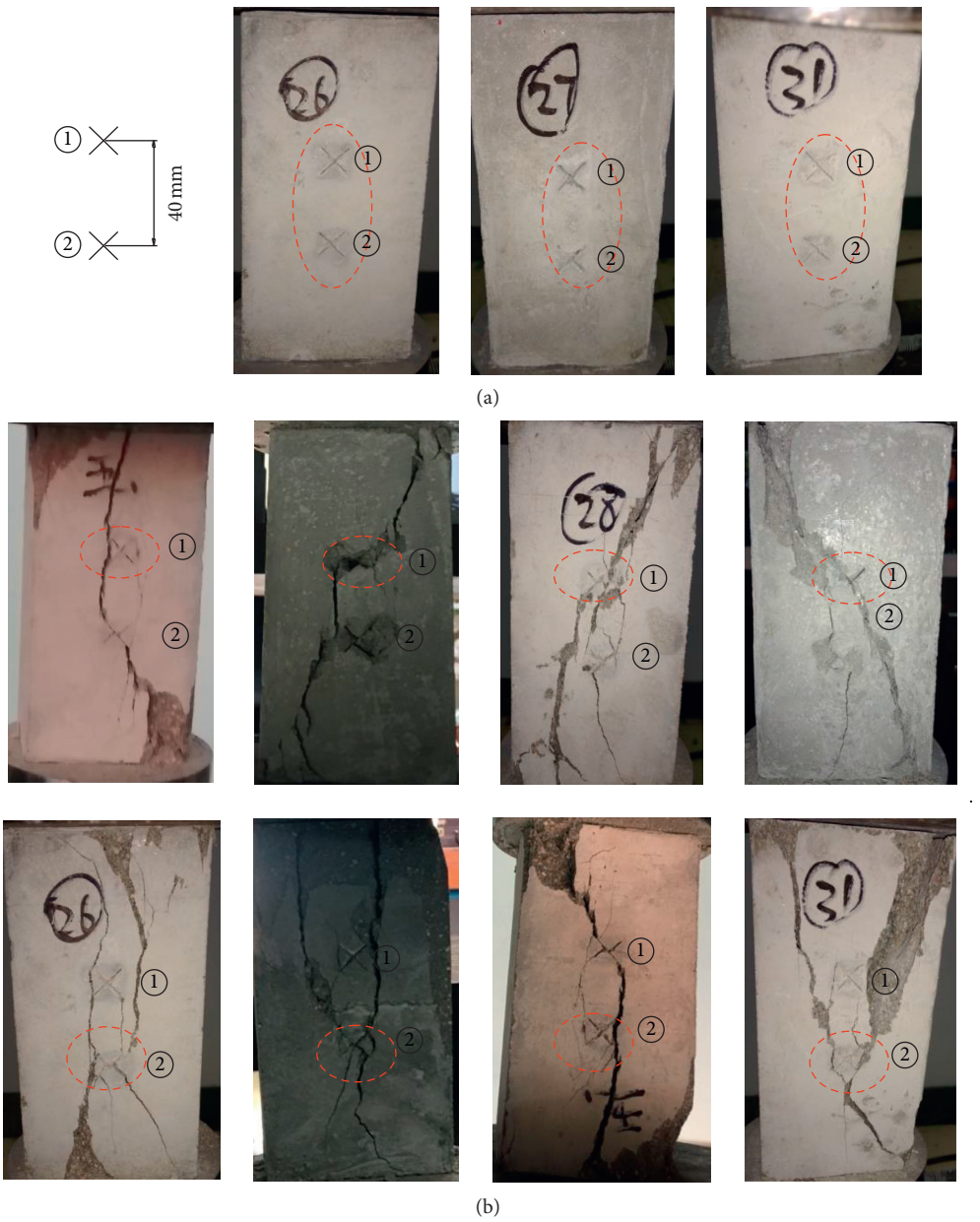

Figure 7: Tests on failure process of rock-like specimens made with double "X" fractures. (a) Sketchy model and parts of rock-like specimens made with double "X" fractures. (b) Failure modes of specimens with double "X" fractures.

their peak strength. When the confining pressure is 10 MPa, there is only one obvious crack and by now, the specimen still has high bearing capacity. When the confining pressure is up to 15 MPa, there is a smaller crack. It demonstrates that the confining pressure can enhance rock's peak strength and inhibit the generation and propagation of cracks.

Excavation disturbance of deep buried cavern leads to the stress redistribution of surrounding rock mass, and its stress state changes from three directions to a bidirectional or even unidirectional state, which results in the dissipation of elastic strain energy with rock masses' crack propagation and discontinuous deformation. In this process, the stress-strain state of rock mass is very complex, and it is difficult to analyze and judge the stability of the surrounding rock mass by only stress or strain state [35–37]. So, on the basis of the above studies, tests on rock masses' unloading effect are analyzed. The test step is as follows: firstly, apply three-dimensional loads on the rock-like specimen, then after all are stable, loading on the larger face of specimen is unloaded to simulate the excavation effect qualitatively (see Figure 11). Test results of specimen's crack propagation pattern are shown in Figure 12.

As seen from Figure 12, when the confining pressure on one face of the specimen is unloaded, the stress on that face is released, and the energy stored in the rock mass is also released in the process of crack propagating.

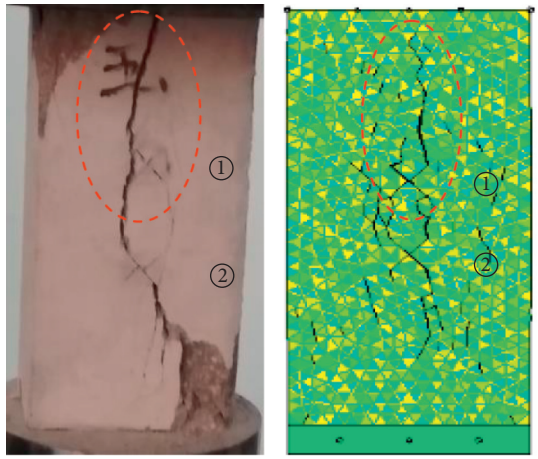

Figure 8: Comparison of test and discontinuous deformation simulation of rock-like specimen made with double "X" fractures.

Figure 9: The triaxial loading machine for rock-like specimen.

Figure 10: Cracking of rock-like specimen with different confining pressures.

Compared with the cracking state without unloading (Figure 10), here, crack propagation is aggravated even under the same confining pressure. At the same time, test results show that crack propagation is mainly parallel to the direction of the maximum principal stress, and this just reveals the cause of the splitting failure in the cavern excavation engineering.

4. Temperature's Influence on Failure Law of Rock-Like Specimen

In order to study the rock crack process at different temperatures, 16 samples with stable sound velocity selected by acoustic emission device are applied on axial compressive loads, and every temperature with four pieces of specimens.

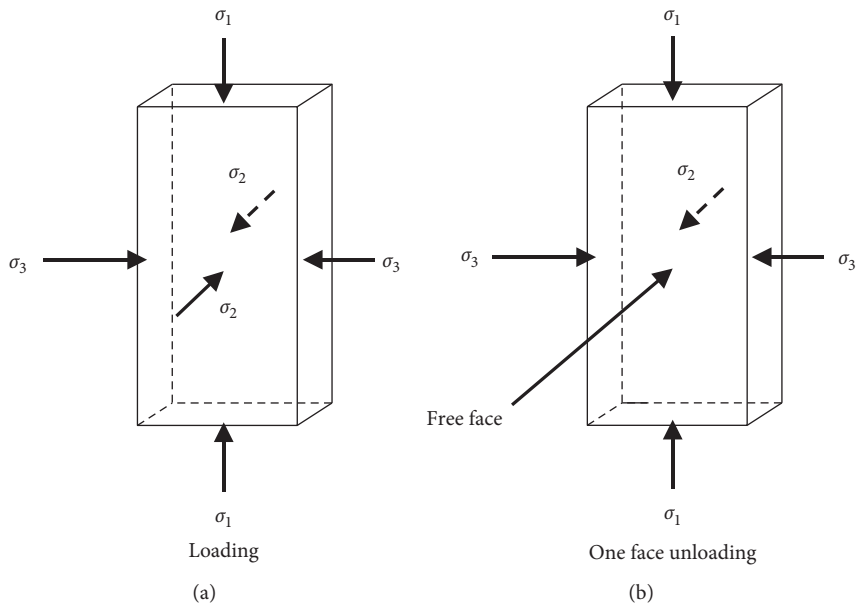

Figure 11: Loading and unloading sketchy diagram of rock-like specimen.

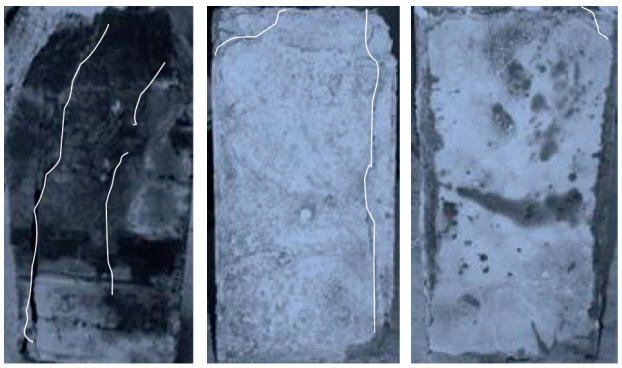

Figure 12: Unloading cracking morphology of rock-like specimens under different confining pressures.

The typical crack morphology of the rock-like specimen after the tests is shown in Figure 13, and their peak strength is shown in Figure 14.

As seen from Figure 13, rock cracking extent increases with the increase of temperature, and the high temperature accelerates energy release stored in the rock and accelerates the process of crack propagation. Therefore, the deeper the rock, the higher the temperature, and it will be more prone to cracking.

As can be seen from Figure 14, the increase of temperature not only accelerates the cracking process of rock mass, but also reduces its strength and bearing capacity significantly. The mean peak strength reduces from 32 MPa (20 degrees Celsius) to 20.4 MPa (80 degrees Celsius), decreasing logarithmically.

In addition, to study relative higher temperature influence on rock masses' cracking, 15 pieces of specimens with similar acoustic velocity are selected to be tested, with 5 pieces of 100°C, 5 pieces of 200°C, and 5 pieces of 300°C. In this compressive test, all specimens of 100°C can be loaded normally until the test is over, while three in five pieces of 200°C are crushed in the loading process and four in five pieces of 300°C are crushed directly in the loading process. The ultimate typical cracking morphologies of eight pieces of specimens can be loaded normally and are shown in Figure 15.

As can be seen from Figure 15, the relative higher temperature can not only reduce the strength of rock mass, but also greatly affect the cracking characteristics. When the temperature is lower, the rock strength is higher, and it has certain compressive strength. As the temperature increases, the peak strength of rock mass decreases (the mean peak strength of rock-like specimen is 19.43 MPa or so at temperature 100°C, the mean peak strength of rock-like specimen is 14.29 MPa or so at temperature 200°C, and the mean peak strength of rock-like specimen is 10.2 MPa or so at temperature 300°C), and it is more likely to crush, which indicates that the disaster of rock burst is more prone to happening under relative higher temperature conditions. Therefore, it is more necessary to strengthen the rock mass under relative higher temperature conditions in the rock engineering.

5. Discussion

Analysis and researches on crack extension have been done preliminarily in this manuscript, including "X" cracks, loading and unloading forces, and different confining pressures and temperatures. Although we select the special analysis points, yet compared with the research progresses both at home and abroad, further studies are needed. Considering the complexity of rock mass engineering, our group will gradually study the hydraulic coupling effects, in order to provide theoretical basis and guidance for rock mass engineering that is rich in water.

t = 20°C t = 40°C t = 60°C t = 80°C

Figure 13: Crack morphology of the rock-like specimen at different temperatures.

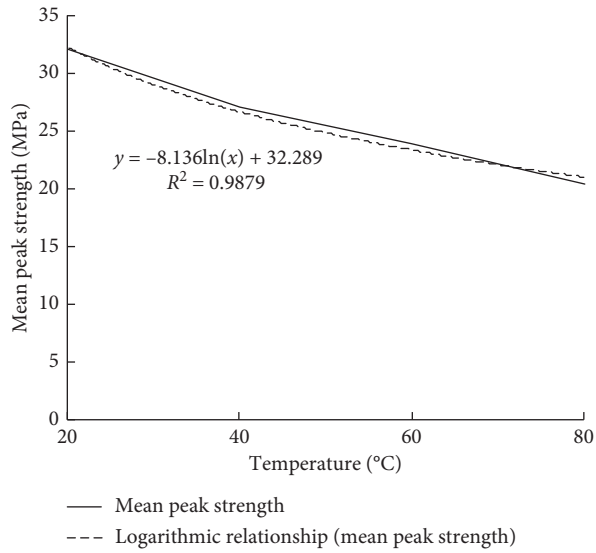

Figure 14: Mean peak strength of the rock-like specimen at different temperatures.

(a) (b) (c)

Figure 15: Crack morphology of specimens at different relative higher temperatures. (a) t = 100°C. (b) t = 200°C. (c) t = 300°C.

6. Conclusions

(1) Through experimental study and discontinuous deformation numerical analysis for rock failure, we can get that one of the two fractures will be taken as the breakthrough point and as the main cracking path for releasing energy for the rock-like specimen with single "X" fracture. And in the same way, for the rock-like specimen with double "X" fractures, one of the two sets of "X" fractures will be selected as the breakthrough set. Therefore, for the rock mass with "X" fractures, in the process of crack propagation, a breakthrough point will always be found, and then a new balance can be reached.

(2) A self-developed hydraulic loading device is used to analyze the confining pressure's influence on rock masses' failure process. This device can apply triaxial loading and also can unload some face. Loading and unloading tests show that the confining pressure can improve the strength of rock mass and restrain the crack propagation. And, the obvious splitting cracks on the unloading surface give the reason why the cave wall is prone to splitting and spalling after excavation.

(3) The higher the temperature, the lower the rock strength, and the more obvious the crack propagation. Under relative higher temperature conditions, rock mass is easier to burst, so, for the rock mass engineering under relative higher temperature condition, the prevention and control of rock burst disaster should be focused on.

Data Availability

All data used to support the findings of this study are available from the corresponding author upon request.

Conflicts of Interest

The authors declare that they have no conflicts of interest.

Authors' Contributions

Methodology and writing-original draft are done by Yunjuan Chen; data curation and software are performed by Yi Jing; supervision is done by Yanchun Yin; writing–review and editing are done by Fuqiang Yin; conceptualization is done by Chenglong Zhao.

Acknowledgments

This study was financially supported by the National Natural Science Foundation of China (No. 51609130), Open Foundation of Key Laboratory of Mining Disaster Prevention and Control by Shandong University of Science and Technology (No. MDPC201909), and Doctoral Foundation of Shandong Jianzhu University (No. XNBS1704).

References

[1] T. Li, X. Pei, D. Wang, R. Huang, and H. Tang, "Nonlinear behavior and damage model for fractured rock under cyclic loading based on energy dissipation principle," *Engineering Fracture Mechanics*, vol. 206, pp. 330–341, 2019.

[2] V. Sarfarazi, H. Haeri, and M. F. Marji, "Numerical simulation of the effect of bedding layer on the tensile failure mechanism of rock using PFC2D," *Structural Engineering & Mechanics*, vol. 69, no. 1, pp. 43–50, 2019.

[3] Q. Zhang, X. Huang, H. Zhu, and J. Li, "Quantitative assessments of the correlations between rock mass rating (RMR) and geological strength index (GSI)," *Tunnelling and Underground Space Technology*, vol. 83, pp. 73–81, 2019.

[4] S. M. R. Niya and A. P. S. Selvadurai, "Correlation of joint roughness coefficient and permeability of a fracture," *International Journal of Rock Mechanics and Mining Sciences*, vol. 113, pp. 150–162, 2019.

[5] R. Kumar and A. K. Verma, "Anisotropic shear behavior of rock joint replicas," *International Journal of Rock Mechanics and Mining Sciences*, vol. 90, pp. 62–73, 2016.

[6] L. A. Le, G. D. Nguyen, H. H. Bui, A. H. Sheikh, A. Kotousov, and A. Khanna, "Modelling jointed rock mass as a continuum with an embedded cohesive-frictional model," *Engineering Geology*, vol. 228, pp. 107–120, 2017.

[7] R. Resende, J. Muralha, A. L. Ramos, and E. Fortunato, "Rock joint topography: three-dimensional scanning and numerical analysis," *Géotechnique Letters*, vol. 5, no. 4, pp. 318–323, 2015.

[8] H. K. Lê, W.-C. Huang, M.-C. Liao, and M.-C. Weng, "Spatial characteristics of rock joint profile roughness and mechanical behavior of a randomly generated rock joint," *Engineering Geology*, vol. 245, pp. 97–105, 2018.

[9] J. Y. Wu, Z. Q. Chen, M. M. Feng et al., "The length of pre-existing fissure effects on the dilatancy behavior, acoustic emission, and strength characteristics of cracked sandstone under different confining pressures," *Environmental Earth Sciences*, vol. 77, no. 12, p. 430, 2018.

[10] Y.-H. Huang, S.-Q. Yang, and W.-L. Tian, "Crack coalescence behavior of sandstone specimen containing two pre-existing flaws under different confining pressures," *Theoretical and Applied Fracture Mechanics*, vol. 99, pp. 118–130, 2019.

[11] Y.-H. Huang and S.-Q. Yang, "Mechanical and cracking behavior of granite containing two coplanar flaws under conventional triaxial compression," *International Journal of Damage Mechanics*, vol. 28, no. 4, pp. 590–610, 2019.

[12] T. Zhu, H. Jing, H. Su, Q. Yin, M. Du, and G. Han, "Physical and mechanical properties of sandstone containing a single fissure after exposure to high temperatures," *International Journal of Mining Science and Technology*, vol. 26, no. 2, pp. 319–325, 2016.

[13] Y.-H. Huang, S.-Q. Yang, and Y.-S. Bu, "Effect of thermal shock on the strength and fracture behavior of pre-flawed granite specimens under uniaxial compression," *Theoretical and Applied Fracture Mechanics*, vol. 106, p. 102474, 2020.

[14] L. L. Li, Y. T. Gao, Y. Zhou et al., "Meso-scale modelling mechanical properties of rock-like material containing trident cracks under uniaxial compression," *Rock and Soil Mechanics*, vol. 39, no. 10, pp. 3668–3676, 2018.

[15] X. W. Liu, Q. S. Liu, B. Liu et al., "Failure behavior for rocklike material with cross crack under biaxial compression," *Journal of Materials in Civil Engineering*, vol. 31, no. 2, pp. 1–8, Article ID 06018025, 2019.

[16] R.-h. Cao, H. Lin, H. Lin et al., "Experimental and numerical study of failure behavior and energy mechanics of rock-like materials containing multiple joints," *Advances in Materials Science and Engineering*, vol. 2017, no. 12, pp. 1–17, 2017.

[17] B. Zhang, S. C. Li, X. Y. Yang et al., "Uniaxial compression tests on mechanical properties of rock mass similar material with cross-cracks," *Rock and Soil Mechanics*, vol. 33, no. 12, pp. 3674–3679, 2012.

[18] B. Zhang, S. C. Li, X. Y. Yang et al., "Bolting effect and failure modes of jointed rock masses with cross-cracks," *Chinese Journal of Rock Mechanics and Engineering*, vol. 33, no. 5, pp. 996–1003, 2014.

[19] B. Zhang, S. C. Li, X. Y. Yang et al., "Mechanical property of rock-like material with intersecting multi-flaws under uniaxial compression," *Chinese Journal of Rock Mechanics and Engineering*, vol. 34, no. 9, pp. 1777–1785, 2015.

[20] B. Zhang, S. C. Li, X. Y. Yang et al., "Uniaxial compression failure mechanism of jointed rock mass with cross-cracks," *Rock and Soil Mechanics*, vol. 35, no. 7, pp. 1863–1870, 2014.

[21] S. Sang, W. Q. Liu, L. Song et al., "On the flow distribution characteristics of cross cracks in rock mass," *Journal of the Society for Experimental Mechanics*, vol. 31, no. 5, pp. 577–583, 2016.

[22] X. C. Li, J. P. Chen, B. F. Shi et al., "A study on the meshless method on seepage of intersected fractures," *Rock and Soil Mechanics*, vol. 28, no. s1, pp. 371–374, 2007.

[23] C. C. Wang, "Experimental study on permeability characteristics of cross fractured rock mass," Master's thesis, Shijiazhuang Railway University, Shijiazhuang, China, 2016.

[24] R. C. Liu, Y. J. Jiang, S. C. Li et al., "Study of nonlinear hydraulic characteristics and hydraulic aperture calculation of crossed fracture," *Rock and Soil Mechanics*, vol. 36, no. 6, pp. 1581–1590, 2015.

[25] Y.-Y. Jiao, X.-L. Zhang, H.-Q. Zhang, H.-B. Li, S.-Q. Yang, and J.-C. Li, "A coupled thermo-mechanical discontinuum model for simulating rock cracking induced by temperature stresses," *Computers and Geotechnics*, vol. 67, pp. 142–149, 2015.

[26] F. Zheng, Y.-Y. Jiao, M. Gardner, and N. Sitar, "A fast direct search algorithm for contact detection of convex polygonal or polyhedral particles," *Computers and Geotechnics*, vol. 87, pp. 76–85, 2017.

[27] X.-L. Zhang, Y.-Y. Jiao, and J.-F. Ma, "Simulation of rock dynamic failure using discontinuous numerical approach," *Computers and Geotechnics*, vol. 96, pp. 160–166, 2018.

[28] C. Yan, Y.-Y. Jiao, and H. Zheng, "A fully coupled three-dimensional hydro-mechanical finite discrete element approach with real porous seepage for simulating 3D hydraulic fracturing," *Computers and Geotechnics*, vol. 96, pp. 73–89, 2018.

[29] P. He, S. C. Li, L. P. Li et al., "Discontinuous deformation analysis of super section tunnel surrounding rock stability based on joint distribution simulation," *Computer and Geotechnics*, vol. 91, pp. 218–229, 2018.

[30] X. Fu, Q. Sheng, Y. Zhang, J. Chen, S. Zhang, and Z. Zhang, "Computation of the safety factor for slope stability using discontinuous deformation analysis and the vector sum method," *Computers and Geotechnics*, vol. 92, pp. 68–76, 2017.

[31] W. Wu, H. Zhu, J.-S. Lin, X. Zhuang, and G. Ma, "Tunnel stability assessment by 3D DDA-key block analysis," *Tunnelling and Underground Space Technology*, vol. 71, pp. 210–214, 2018.

[32] Y. Zhang, Q. Xu, G. Chen, J. X. Zhao, and L. Zheng, "Extension of discontinuous deformation analysis and application in cohesive-frictional slope analysis," *International Journal of Rock Mechanics and Mining Sciences*, vol. 70, pp. 533–545, 2014.

[33] Y. B. Gony and H. H. Yossef, "Benchmarking the numerical discontinuous deformation analysis method," *Computer and Geotechnics*, vol. 71, pp. 30–46, 2016.

[34] F. Zheng, Y. F. Leung, J.-B. Zhu, and Y.-Y. Jiao, "Modified predictor-corrector solution approach for efficient discontinuous deformation analysis of jointed rock masses," *International Journal for Numerical and Analytical Methods in Geomechanics*, vol. 43, no. 2, pp. 599–624, 2019.

[35] Z. Wang, D. R. Schmitt, W. Zhou, R. Wang, Y. Zang, and Y. Zeng, "Removed: the stress dependence of velocities and its influencing factors for carbonate rocks in Arab formation, Saudi Arabia," *Journal of Petroleum Science and Engineering*, vol. 173, pp. 1368–1381, 2019.

[36] K. A. Arash, K. Bijay, F. Maziar et al., "Stress-strain response and seismic signature analysis of phyllite reservoir rocks from Blue Mountain geothermal field," *Geothermics*, vol. 77, pp. 204–223, 2019.

[37] F. Wang and J. F. Zou, "A simple prediction procedure of strain-softening surrounding rock for a circular opening," *Geomechics and Engineering*, vol. 16, no. 6, pp. 619–626, 2018.